OXFORD
SOT | Society of Toxicology
academic.oup.com/toxsci

Toxicological Sciences, 2023, **191(2),** 285–295
https://doi.org/10.1093/toxsci/kfac125
Advance Access Publication Date: 2 December 2022
Research article

Cellular and molecular responses to ethyl-parathion in undifferentiated SH-SY5Y cells provide neurotoxicity pathway indicators for organophosphorus impacts

Saroj K. Amar,[1,2] Keri B. Donohue,[2] Kurt A. Gust [2,*]

[1]Oak Ridge Institute for Science and Education, Oak Ridge, Tennessee 37830, USA
[2]US Army, Engineer Research and Development Center, Environmental Laboratory, Vicksburg, Mississippi 39180, USA
Disclaimer: Views expressed in this article are those of the authors and do not necessarily reflect official policy or position of the Department of the Army, Department of Defense, nor the U.S. Government. This work was prepared as part of official duties by employees of the U.S. Government.

*To whom correspondence should be addressed at US Army, Engineer Research and Development Center, Environmental Laboratory EPP, 3909 Halls Ferry Rd, Vicksburg, MS 39180, USA. E-mail: kurt.a.gust@usace.army.mil.

Abstract

High-fidelity nonanimal screening methods are needed that can rapidly and accurately characterize organophosphorus compound (OP)-induced neurotoxicity. Herein, the efficacy of human neuroblastoma cell line (SH-SY5Y) to provide molecular and cellular responses characteristic of the OP neurotoxicity pathway was investigated in response to the OP-model compound, ethyl-parathion. Undifferentiated SH-SY5Y cells were exposed to ethyl-parathion for 30 min at 0 (control), 0.5, 2.5, 5, 10, and 25 μg/ml. Dose-responsive reductions in cell viability were observed with significant reductions at ≥10 μg/ml. From these results, ethyl-parathion exposures of 0 (control), 5, and 10 μg/ml were selected to examine bioindicators underlying the OP neurotoxicity pathway including: reactive oxygen species (ROS), cell membrane peroxidation, mitochondrial membrane potential (MMP), and apoptosis. Ethyl-parathion elicited highly significant increases in ROS relative to controls ($p < .01$) at both exposure concentrations, confirmed using N-acetyl cysteine (NAC) as a ROS quencher which alleviated ROS increases. A response characteristic of increased ROS exposure, cell membrane-lipid peroxidation, significantly increased ($p < .05$) at the highest ethyl-parathion exposure (10 μg/ml). As a likely consequence of membrane-lipid peroxidation, ethyl-parathion-induced reductions in MMP were observed with significant effects at 10 μg/ml, reducing MMP by 58.2%. As a culmination of these cellular-damage indicators, apoptosis progression was investigated by phosphatidylserine translocation where ethyl-parathion-induced dose-responsive, highly significant ($p < .01$) increases at both 5 and 10 μg/ml. Overall, the mechanistic responses observed in undifferentiated SH-SY5Y cells corresponded with *in vivo* mammalian results demonstrating potential for this nonanimal model to provide accurate OP neurotoxicology screening.

Keywords: neurotoxicity; ethyl-parathion; reactive oxygen species; mitochondrial membrane potential; lipid peroxidation.

The organophosphorus class of compounds (OP) are widely used in agriculture as insecticides and acaricides, the release of which may result in hazardous occupational and public exposures (Argentin *et al.*, 2015). The acute toxicological mechanism of action for OPs in humans involves inhibition of acetylcholinesterase (AChE) causing hyper-excitation of the cholinergic nervous system, respiratory paralysis, and possible death (Namba, 1971). Sublethal manifestations of acute and/or chronic exposures to OPs include impaired memory and concentration, disorientation, severe depression, irritability, confusion, headache, speech difficulties, delayed reaction time, nightmares, sleepwalking, and drowsiness (USEPA, 2000). Underlying these neurological impairments, OPs cause a cascade of cellular events leading to neurotoxicity and neurodegeneration (Canales-Aguirre *et al.*, 2012). In neurons, the stimulation of cholinergic and glutamatergic signaling pathways by OPs elicits the production of reactive oxygen species (ROS) disrupting mitochondrial function in a positive feedback loop that further expands ROS release and calcium release into cells which ultimately induces apoptosis mechanisms leading to cell death (Farkhondeh *et al.*, 2020). The ability to mechanistically connect these neuronal cell responses to whole-organism neurotoxicity in OP exposures is clearly needed to enable the development of nonanimal screening technologies for predicting OP impacts and serve as a testbed for developing protective or therapeutic countermeasures to OP neurotoxicity.

Presently, the investigation of neurotoxicity and neurodegenerative disease progression is largely dependent on research methods that use animal models. Replacement of animal models remains a high priority within the toxicology community of practice, and molecular mechanisms-based approaches for understanding toxicological pathways (Ankley *et al.*, 2010; Gust *et al.*, 2019, 2020) hold promise for providing nonanimal assays that provide high-fidelity assessment (Judson *et al.*, 2010; Richard *et al.*, 2016). In the present study, we sought to determine the efficacy of *in vitro* cell-based assays to recapitulate fundamental mechanistic neurotoxicity responses to OPs observed *in vivo*. Specifically, we utilized the undifferentiated human

neuroblastoma cell line, SH-SY5Y, which exhibits characteristic acetylcholine (ACh) signaling (Heusinkveld and Westerink, 2017), retains both muscarinic and nicotinic acetylcholine receptors (Kovalevich and Langford 2013), has inherent dopaminergic properties (Heusinkveld and Westerink, 2017; Kovalevich and Langford, 2013), and has been used extensively for *in vitro* neurotoxicity study (Faria *et al.*, 2016; Sala *et al.*, 2016) as our cellular target for this investigation. Ethyl-parathion was selected as the OP model compound, where in previous *in vitro* exposures in undifferentiated fetal rat neuronal cells (Monnet-Tschudi *et al.*, 2000), it was 24 times more potent at inhibiting AChE activity than the OP-compound, chlorpyrifos, and was similarly effective at AChE inhibition (within a factor of 4) of the less-stable activated oxon derivative, paraoxon. Ethyl-parathion represents an active-use pesticide in developing nations, and both cellular and molecular endpoints involved in the OP neurotoxicity pathway were investigated in the undifferentiated SH-SY5Y cells. Charting the OP neurotoxicity pathway, we investigated oxidative stress, lipid peroxidation, mitochondrial function, and progression of cellular apoptosis targeting both sub-lethal and lethal ethyl-parathion concentrations. Finally, we compared these *in vitro* responses in SH-SY5Y cells to literature-based observations of OP effects in *in vivo* exposures to establish correspondence in responses and provide conclusions on the efficacy of these *in vitro* assays to provide relevant mechanistic insights.

Materials and methods

Chemicals and media

The following chemicals and reagents used in the experimental investigations were purchased from Sigma Chemical Co (St. Louis, Missouri): ethyl-parathion (45607-100MG), purity ≥98.0%, 2–7 dichlorofluorocene di-acetate (H_2DCFDA, D6883-50G), N-acetyl L-cysteine (NAC, A7260-10G), fetal bovine serum (F2442), Dulbecco's Modified Eagle's Medium/Nutrient Mixture F12 Ham's (DMEM/F-12, D6421-500ML), penicillin-streptomycin solution (P4333-100ML), trypsin (0.25%, T4424-500M), 3-(4,5-dimethylthiazol-2-yl)-2,5-diphenyltetrazolium bromide (MTT, M2128-250MG), trichloroacetic acid (T6399-100G), ethidium bromide (E1385-5ML), acridine orange (318337-1G), annexin-V, fluorescein isothiocyanate conjugate (FITC) (A9210-20TST), propidium iodide (P2667-20TST), Hank's balanced salt solution (HBSS, H4891-10X1L), and dimethyl sulfoxide (DMSO) (276855-1L). Tetraethylbenzimidazolylcarbocyanine iodide (JC-1, 420200-5MG) was purchased from Millipore (Millipore Corporation). The SH-SY5Y human neuronal cells were purchased from American Type Culture Collection (CRL-2266, ATTC, Manassas, Virginia) in addition to Eagle's Minimum Essential Medium (ATCC 30-2003). Trypan blue stain (ref no. 15250-061) and phosphate saline buffer (PBS, ref no. 70011044) were purchased from Gibco, Life Technologies Inc (Thermo Fisher Scientific, Waltham, Massachusetts). High-capacity cDNA reverse transcription kit (ref no. 4368814) and SYBR green PCR master mix (ref no. 4309155) were purchased from Applied Biosystem, Life Technologies (Thermo Fisher Scientific). RNeasy Mini Kits (Cat no. 74104) were purchased from Qiagen (Qiagen, Hilden, Germany). Finally, 4′,6-diamidino-2-phenylindole (DAPI, ref no. D3571) and nuclease-free water (AM9932) were purchased from Ambion, Life Technologies Inc (Thermo Fisher Scientific).

Cell culture

Human neuronal cells SH-SY5Y received from ATCC were of passage number 28. The vial of frozen SH-SY5Y cells was thawed and cells were cultured at 37°C in a CO_2 incubator with 5% CO_2. Cells were cultured with DMEM/F-12 and Eagle's Minimum Essential Medium cell culture medium (1:1), supplemented with 10% heat inactivated FBS and penicillin streptomycin solution (1%). Culture media was renewed every 24 h. The SH-SY5Y cells were not differentiated using retinoic acid, tetradecanoylphorbol acetate, or any other chemical inducers; therefore, the cells retained a state similar to immature catecholaminergic neurons (Kovalevich and Langford, 2013). Importantly, undifferentiated SH-SY5Y cells express muscarinic and nicotinic acetylcholine receptors with G-protein coupled receptors present on cellular membranes as well as intact dopaminergic neuronal markers (Kovalevich and Langford, 2013), which are critical for pathway-level for understanding OP neurotoxicity.

Cell viability/cytotoxicity assay

Cell viability was determined using the MTT assay according to the standard test protocol of Mosmann (1983). In brief, 1×10^4 cells were plated in each well of 96-well plates and incubated in the 5% CO_2 incubator at 37°C to reach approximately 70–80% confluency within 25–48 h. The cells were then exposed to ethyl-parathion in water at 0 (control), 0.5, 2.5, 5, 10, and 25 μg/ml concentrations (3 replicates per dose). The ethyl-parathion solution was adminstered to the cells (for this assay and all additional assays described in sections "Estimation of intracellular ROS generation, Parathion-induced malondialdehyde (MDA) formation, Measurement of mitochondrial membrane potential, Ethidium bromide/acridine orange (EB/AO) apoptotic assay, Phosphatidylserine (PS) translocation, and Image capture and analysis") and subsequently incubated for 30 min. After incubation, cells were washed twice with HBSS and replaced by MTT (5 mg/ml) in 200 μl complete medium. The culture plates were incubated in the CO_2 incubator for 4 h. After incubation, the culture plates were washed twice with HBSS and 200 μl of DMSO was added to each well by pipetting up and down to dissolve the formazan crystals. Spectral absorbance of formazan was recorded at 570 nm using a Biotek multi-well microplate reader (Agilent Technologies, Santa Clara, California).

Estimation of intracellular ROS generation

Cells were plated as described in section "Cell viability/cytotoxicity assay" and then treated with 0 (control), 5, and 10 μg/ml of ethyl-parathion including 4 replicates per dose. Ethyl-parathion exposures were conducted for 30 min at 37°C with 5 μM carboxy-H_2DCF-DA in the HBSS exposure medium. After incubation, the fluorescence intensity of DCF was measured using a Biotek microplate reader (Agilent Technologies) using 480 nm excitation and 530 nm emission wavelengths. The generation of intracellular ROS was further validated by adding 100 μg/ml of NAC to act as a ROS quencher (Zhao *et al.*, 2016) in the 10 μg/ml ethyl-parathion exposure treatment (4 replicates).

Parathion-induced malondialdehyde (MDA) formation

A total of 2.25×10^6 cells were seeded in 100 mm cell culture dishes and allowed to reach approximately 70–80% confluency within 25–48 h. The cells were then treated with 0 (control), 5, and 10 μg/ml of ethyl-parathion in water (3 replicates per dose) for 30 min. The cells were then scraped in 2.5% trichloroacetic acid (TCA) and homogenized. After centrifugation at 1107 g for 5 min at 4°C, supernatant was added with 0.5% (w/v) TCA and incubated in a water bath at 95°C for 30 min. The supernatant was then cooled in an ice bath and then spectral absorbance of supernatant was recorded at 532 and 600 nm using a Biotek

multi-well microplate reader (Agilent Technologies). Based on these observations, MDA as final product of lipid peroxidation was calculated using extinction co-efficient 155 $mM^{-1} cm^{-1}$ (Goyal *et al.*, 2016).

Measurement of mitochondrial membrane potential

Mitochondrial transmembrane potential (MTP) was assessed with fluorescent chromophores probe JC-1 and DAPI (4′, 6-diamidino-2-phenylindole). Cells were labeled by DAPI to visualize nuclei and JC-1 to visualize mitochondria as described in (Piña-Guzmán *et al.*, 2009). The lipophilic cationic dye, JC-1, selectively enters healthy mitochondria with high transmembrane potential and accumulates as J-aggregates and emitting red fluorescence. Simultaneously, if the transmembrane potential collapses in damaged mitochondria, the JC-1 dye can no longer accumulate and remains in the cytoplasm in a monomeric form that emits green fluorescence (Piña-Guzmán *et al.*, 2009). A total of 3×10^5 cells were seeded into 6-well plates and allowed to reach approximately 70–80% confluency within 25–48 h. The cells were then treated with ethyl-parathion in water at 0, 5, and 10 μg/ml for 30 min (4 replicates per dose). The MTP reagent cocktail was prepared with 5 μM of JC-1 and 0.1 μg/ml of DAPI. Immediately following the ethyl-parathion exposure, cells were incubated with the JC-1/DAPI cocktail for 30 min in dark at 37°C, washed and images were visualized using an EVOS 5000 cell imaging system (Thermo Fisher Scientific) using green fluorescent protein (GFP), red fluorescent protein (RFP), and DAPI (blue-fluorescent) filters following the methods described in section "Image capture and analysis".

Ethidium bromide/acridine orange (EB/AO) apoptotic assay

A cocktail (1:1) of ethidium bromide (EB) (10 μg/ml) and acridine orange (AO) (100 μg/ml) was prepared in PBS. Cells were plated as described in section "Measurement of mitochondrial membrane potential" and then exposed to ethyl-parathion in water at 0, 5, and 10 μg/ml (4 replicates per treatment) for 30 min. Immediately following ethyl-parathion exposure, cells were washed twice with PBS, and then fresh medium was added. After an additional 6 h of incubation, cells were washed again with PBS and stained with the EB/AO cocktail and kept for 30 min at 37°C. Cells were washed with PBS and analyzed with fluorescent microscope using GFP and RFP filters for EB and AO respectively using the EVOS 5000 cell imaging system (Thermo Fisher Scientific).

Phosphatidylserine (PS) translocation

Cells were plated as described in section "Measurement of mitochondrial membrane potential" and then treated with ethyl-parathion in water at 0, 5, and 10 μg/ml (4 replicates per exposure) for 30 min. Immediately following ethyl-parathion exposure, cells were then stained with the cocktail of Annexin V-FITC conjugate (5 μl/ml) and propidium iodide (10 μl/ml) prepared in binding buffer (A9210-1X Sigma). Annexin V binds phosphatidylserine (PS), which during apoptosis is translocated to the outer leaflet of the cellular membrane (Audo *et al.*, 2017). After incubation for 30 min at 37°C, fluorescence was detected using the EVOS 5000 cell imaging system (Thermo Fisher Scientific) with GFP and RFP filter for Annexin V-FITC and propidium iodide (PI), respectively (Amar *et al.*, 2015; Brauchle *et al.*, 2014). Use of propidium iodide (PI) and fluorescein isothiocyanate (FITC)-conjugated annexin V (Annexin V-FITC) is a standard procedure to monitor the progression of cellular apoptosis. This assay discriminates early and late-stage apoptotic processes in the cell population. In early-stage apoptosis, phospholipid asymmetry is disrupted leading to the exposure of PS on the outer leaflet of the cytoplasmic membrane but in late-stage apoptosis, PS translocation as well as PI staining of the nucleus is present. As described in Brauchle *et al.* (2014) early apoptotic cells are annexin V-positive and PI-negative (annexin V-FITC+/PI−), whereas late (end-stage) apoptotic cells are annexin V/PI-double-positive (annexin V-FITC+/PI+). The early- and late-stage apoptotic populations were manually scored simultaneously for FITC and PI channels in fluorescence mode post-acquisition by fluorescence imaging using the EVOS 5000 cell imaging system.

Image capture and analysis

The methods described in this section provide the approach used to capture images and extract cellular-level data connected with the assays described in sections "Measurement of mitochondrial membrane potential, Ethidium bromide/acridine orange (EB/AO) apoptotic assay, and Phosphatidylserine (PS) translocation". In each assay, a total of 4 images were captured from randomly selected microscopic fields within each of 4 replicate cell plates. All images for each assay were captured using a uniform magnification and scale bar for all replicates. To quantify specific fluorescence signals within the cell images, ImageJ Software (National Institutes of Health, Schneider *et al.*, 2012) was used to separate and quantify each dye-specific signal channel. Each image was first corrected for signal background using image-wide background normalization and this process was repeated for each signal channel. To determine the percent of cells in each stage of apoptosis (section "Phosphatidylserine (PS) translocation"), a minimum of 100 cells were manually counted per image where early or late apoptotic stage classification was determined based on the characteristic fluorescence labeling observations. For all image analyses, mean values were calculated for the 4 images examined per replicate and these mean values per replicate were used for statistical analyses (statistical methods described below).

Transcriptional expression for genes involved in apoptosis and neurotoxicity

Reverse-transcriptase quantitative real-time polymerase chain reaction (RT-qPCR) analysis was used to investigate transcriptional expression for genes involved in apoptosis and neurotoxicity. Expression for a set of 8 target gene transcripts was investigated relative to a constitutive control (ACTB-actin beta), where gene identities and corresponding primer sets developed and ordered from Integrated DNA Technologies, Inc (Coralville, Iowa) are provided in Table 1. Cells were plated as described in section "Parathion-induced malondialdehyde (MDA) formation" and then treated with ethyl-parathion in water at 0, 5, and 10 μg/ml (3 replicates per treatment) for 30 min. Cells were collected immediately after the ethyl-parathion exposure and total RNA was isolated using RNeasy mini kit (Qiagen) according to manufacturer's protocol. Isolated RNA concentration was measured and quality assured using a DS-11+ spectrophotometer (DeNovix Inc, Wilmington, Delaware). RNA samples were converted to copy DNA (cDNA) using Applied Biosystems high-capacity cDNA reverse transcription kit (Thermo Fisher Scientific). The resulting cDNA was quantified by DS-11+ spectrophotometer. The RT-qPCR experiments were conducted using Applied Biosystems SYBR green PCR assays (Thermo Fisher Scientific). RT-qPCR assays were completed using an Applied Biosystems, QuantStudio 7 Flex (Thermo Fisher Scientific). Relative quantification using the ΔΔCT method was applied where transcriptional expression was normalized to the beta-actin housekeeping gene

Table 1. Identity of reverse-transcriptase quantitative PCR (RT-qPCR) gene-transcript targets including target gene symbols, accession numbers, and forward and reverse primer sequences

Gene symbol	Accession number	Forward primer sequence	Reverse primer sequence
CYP4502E1	NM_000773.4	GCAACCCGAGACACCATTTT	GCACACACTCGTTTTCCTGT
MAPK-14	NM_001315.3	CAGTGGGATGCATAATGGCC	GCATCTTCTCCAGCAAGTCG
BAX	NM_001291428.2	AAGAAGCTGAGCGAGTGTCT	GTTCTGATCAGTTCCGGCAC
CYTC	NM_018947.6	AGCAGAGGACTTGGTGACTG	AAACGCCACAACTAGCCAAG
BCL2	NM_000633.3	CCTCGCTGCACAAATACTCC	TGGAGAGAATGTTGGCGTCT
ACTB	NM_001101.5	CATCCGCAAAGACCTGTACG	CCTGCTTGCTGATCCACATC
TH	NM_000360.4	CAGTTCTCGCAGGACATTGG	CTGGTACGTCTGGTCTTGGT
DAT (SLC6A3)	NM_001044.5	TGTGCCCATGAGTAAGAGCA	AAGTCGATCTTCTTGCCCCA
VMAT (SLC18A2)	NM_003054.6	CCGTACATCCTCATTGCTGC	CCACCTCCCCATTTTGTGTG

and then fold change values were calculated relative to controls (Livak and Schmittgen, 2001).

Statistical analysis

The effects of ethyl-parathion exposures were investigated using 1-way analysis of variance (ANOVA) followed by Dunnett's pairwise test against the control (0 μg/ml). Assumptions of ANOVA were tested where normality was investigated using Shapiro-Wilk test and equality of variance assessed using the Brown-Forsythe test. In events where data did not meet the assumptions of ANOVA the data were $\log_{10}$ transformed and analyzed, and if still not meeting the assumptions of ANOVA, analyzed using ANOVA on ranks. The test of ROS quenching by application of NAC in the 10 μg/ml ethyl-parathion exposures was analyzed using a Mann-Whitney *t*-test comparing the 10 μg/ml ethyl-parathion treatment versus the 10 μg/ml ethyl-parathion + 100 μg/ml NAC treatment. This analysis flow was used for all experimental data, including the RT-qPCR data. All statistical tests were executed using SigmaPlot/SigmaStat v. 13.0 (Systat Software, Inc, San Jose, California).

Results

Ethyl-parathion-induced reduction of cell viability

Cytotoxic effects of ethyl-parathion to undifferentiated SH-SY5Y cells were observed with cell viability decreasing with increasing ethyl-parathion concentration (Figure 1). Cell viability decreased significantly in the 10 and 25 μg/ml exposures relative to controls (0 μg/ml). These results were used to select 5 μg/ml as a representative sublethal ethyl-parathion exposure and 10 μg/ml as an exposure which initiated a significant lethal response for use in all the following cell-based assays.

Ethyl-parathion-induced generation of intracellular ROS

Significant increases in ROS, as measured by DCF fluorescence intensity, were identified in the 5 and 10 μg/ml ethyl-parathion exposed undifferentiated SH-SY5Y cells relative to controls (Figure 2). ROS generation in the ethyl-parathion exposure was confirmed by addition of 100 μg/ml N-acetyl cysteine (NAC) to the 10 μg/ml ethyl-parathion exposure which significantly reduced the DCF fluorescent intensity, and thus served to mitigate ROS generated in the ethyl-parathion exposure (Figure 2).

Ethyl-parathion-induced lipid peroxidation

A significant increase in lipid peroxidation, as indicated by MDA level (an end-product of lipid peroxidation), was observed in the 10 μg/ml ethyl-parathion-treated undifferentiated SH-SY5Y cells compared with the controls (Figure 3).

Ethyl-parathion-induced loss of mitochondrial membrane potential

Exposure to ethyl-parathion caused dose-responsive reductions in mitochondrial membrane potential (MMP) where the membrane potential was significantly reduced in the 10 μg/ml exposure (Figure 4) as indicated by an overall red to green shift in fluorescence of JC-1 dye with increasing ethyl-parathion concentration. The ratio of red to green fluorescence was less than half of the control in the 10 μg/ml exposure.

Ethyl-parathion-induced apoptosis

Morphological staining assays differentiated viable and apoptotic cells on the basis of plasma membrane integrity (EB staining) as well as chromatin integrity (AO staining). EB/AO staining indicated significantly increased apoptosis in ethyl-parathion exposures versus controls (Figure 5). Specifically, cells exposed to ethyl-parathion at 5 and 10 μg/ml showed significantly increased red fluorescence, which indicates damage of plasma membranes (Figure 5) given that EB selectively stains cells that have lost membrane integrity. The shifting ratio of green to red fluorescence demonstrated that the control cells (0 μg/ml) were healthy, the 5 μg/ml ethyl-parathion exposed cells were likely in early apoptosis stages, whereas the 10 μg/ml ethyl-parathion exposed cells were likely in late stages of apoptosis.

Validation of early- and late-stage apoptosis in ethyl-parathion exposures

Immunofluorescence investigations identified early- and late-apoptotic cells on the basis of translocation of PS from inner to outer leaflet of plasma membrane by Annexin V-FITC and PI staining (Figure 6). Based on the assay results, the 5 μg/ml ethyl-parathion exposure caused significantly increased translocation of PS from inner to outer leaflet of plasma membrane which is indicative of early-stage apoptosis as detected through annexin V staining. Cells exposed to parathion at 10 μg/ml displayed significantly increased numbers at late apoptotic stages as shown by fluorescence of both annexin V and PI staining (Figure 6).

Ethyl-parathion-induced mRNA expression of apoptotic and neurotoxic genes

Ethyl-parathion caused significant transcriptional expression changes in only one transcript compared with the controls, DAT, which had significantly increased relative expression (Figure 7). Trends of increased transcriptional expression in the ethyl-parathion exposures relative to controls were observed for BAX, BCL2, CYTC, and CYP450 2E1; however, these increases were not statistically significant. The *t*-tests comparing expression in 10 μg/ml ethyl-parathion exposures before and after 100 μg/ml NAC treatment demonstrated significant reductions in

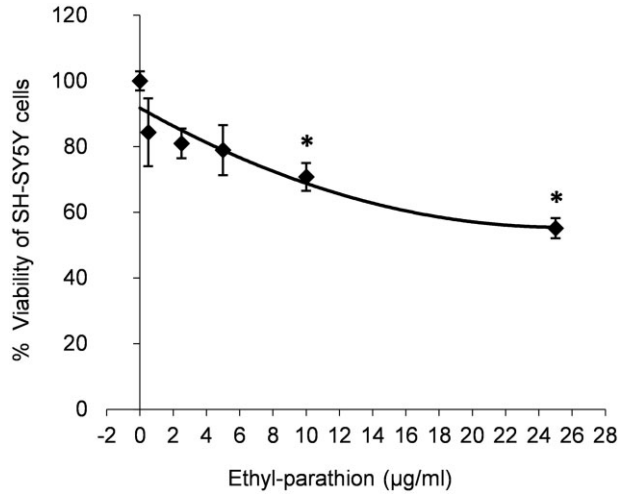

Figure 1. Viability of human neuronal cells SH-SY5Y in response to 30-min ethyl-parathion exposures as determined by MTT assay. The % viability data were calculated relative to control cells (0 µg/ml ethyl-parathion) where points represent means and error bars represent standard error. Significance values are represented as follows: "*" for $p = .05$.

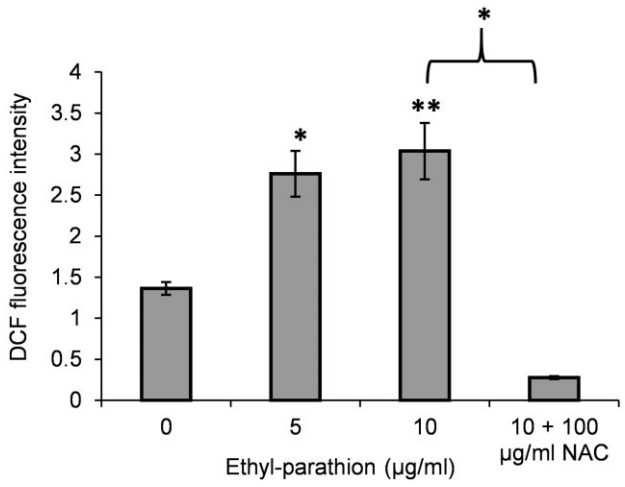

Figure 2. Intracellular reactive oxygen species (ROS) generation in response to ethyl-parathion exposure as indicated by DCF fluorescence in SH-SY5Y cells. Vertical bars represent mean values, whereas error bars represent standard error. N-acetyl L-cysteine (NAC) was used as ROS scavenger which was applied to the 10 µg/ml ethyl-parathion exposure. The Mann-Whitney rank sum test of fluorescence among the 10 µg/ml ethyl-parathion and 10 µg/ml ethyl-parathion + 100 µg/ml NAC treatments was statistically significant, as indicated by the bracket among treatments (Y axis represents in millions). Significance values are represented as follows: "*" for $p = .05$ and "**" for $p = .01$.

transcriptional expression for BAX, BCL2, CYTC, and VMAT post-NAC treatment (Figure 7).

Discussion

Ethyl-parathion effects on cell viability

The OP model compound, ethyl-parathion-induced cytotoxicity in undifferentiated SH-SY5Y cells that was dose-dependent, with significant decreases in viability relative to controls at 10 and 25 µg/ml (Figure 1) after exposure for only 30 min. In comparison, Bharate *et al.* (2010) demonstrated that SH-SY5Y cells exposed to methyl-parathion exhibited decreased viability relative to

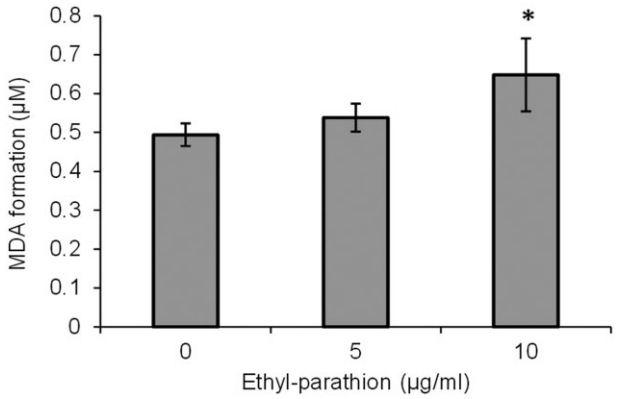

Figure 3. Parathion-induced lipid peroxidation in SH-SY5Y cells as determined by melondialdehyde (MDA) formation as the end product of lipid membrane peroxidation. Vertical bars represent means and error bars represent standard error. Significance values are represented as follows: "*" for $p = .05$.

controls at 100 µM (26.3 µg/ml) and 50 µM (13.2 µg/ml), but only after 24 and 48 h of continuous exposure, respectively. The OP pesticide chlorpyrifos, which has a different molecular structure relative to parathion-based compounds exhibited dose-responsive decreases in viability which were initiated at 25 µg/ml relative to controls in 24 h exposures (Dai *et al.*, 2015). These results indicate that the ethyl-substituted parathion molecular structure induces cytotoxicity in SH-SY5Y cells at comparable effective concentrations as methyl-parathion and chlorpyrifos, but in much shorter duration exposures. This suggests increased relative potency of ethyl-parathion in SH-SY5Y cells in comparison to these other OP compounds, but definitive potency comparison requires further testing using a single exposure duration and a common set of experimental methods among all chemical exposures.

ROS induction

Our results identified significant increases in ROS generation in undifferentiated SH-SY5Y cells exposed for 30 min to ethyl-parathion at 5 and 10 µg/ml, a result that was confirmed by significant quenching of the oxidative stress by administration of NAC (Figure 2). Pesticide-induced ROS generation in SH-SY5Y cells has previously been observed using DCFDA assays when examining known dopaminergic neurotoxic pesticides including dinoseb, rotenone, and imazalil (Heusinkveld and Westerink, 2017). Whole-organism responses in chronic *in vivo* inhalation exposures to parathion identified oxidative stress as the causative mechanism for neurodegenerative damage in rat brains (Canales-Aguirre *et al.*, 2012). Further, markers of oxidative stress have also been observed in occupational exposures to workers involved in OP pesticide manufacturing (Ranjbar *et al.*, 2002). Overall, the observation of ethyl-parathion-induced ROS generation in the SH-SY5Y cells provides a cellular response that is consistent with whole-organism and occupational responses of concern for neurotoxic effects.

Lipid peroxidation

Next, we investigated potential ROS-related damage to membrane lipids which are prone to oxidative damage (Mylonas and Kouretas, 1999). The lipid peroxidation end-product, MDA, increased significantly relative to controls in SH-SY5Y cells exposed to ethyl-parathion at 10 µg/ml (Figure 3). MDA formation

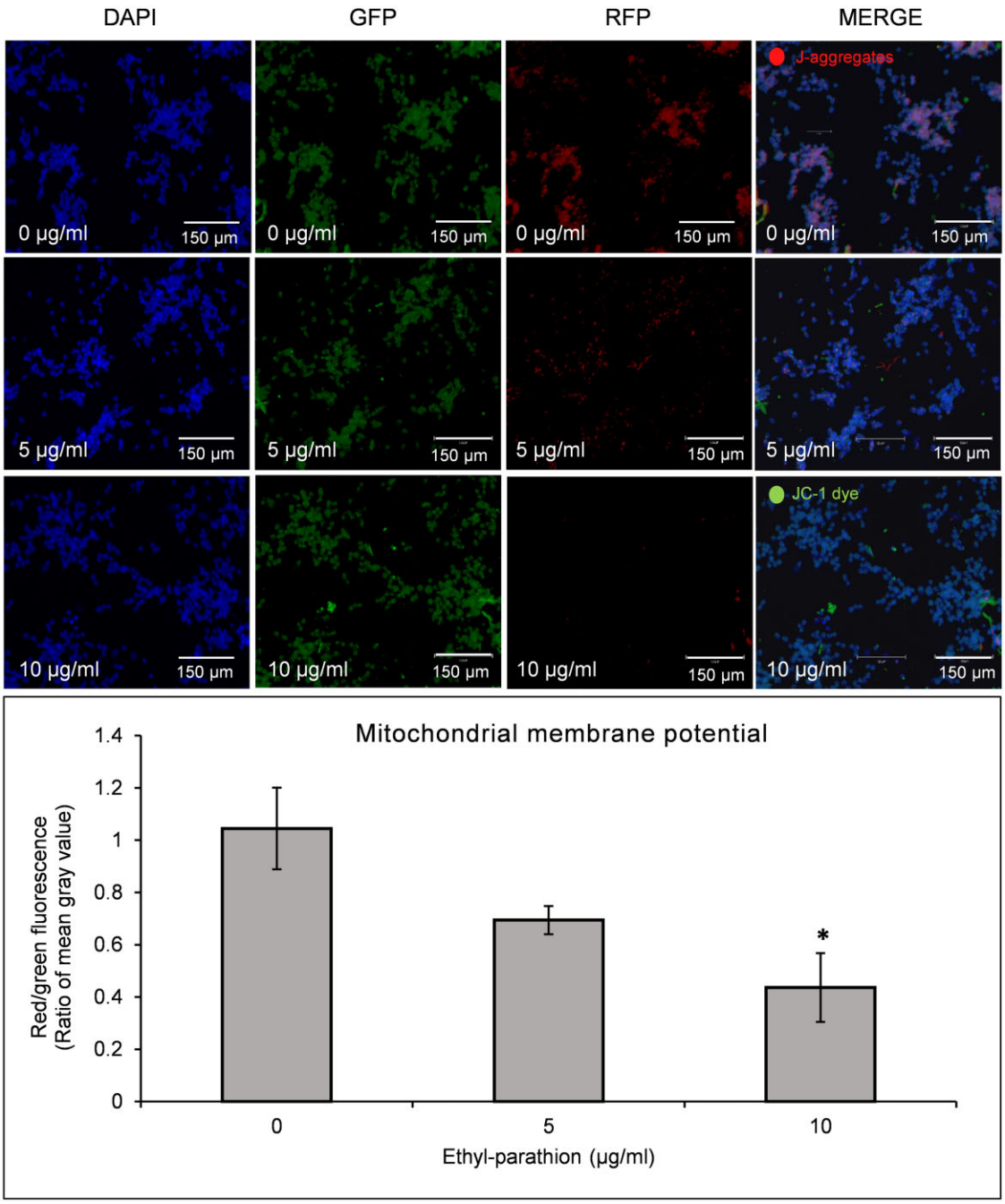

Figure 4. Effect of ethyl-parathion exposure on mitochondrial membrane potential as indicated by JC-1 staining in SH-SY5Y cells. DAPI filter indicates DAPI nuclear staining, whereas GFP/RFP filter indicates JC-1 staining with RFP indicating healthy mitochondrial membranes and GFP indicating unhealthy membranes. Scale bar on image: 150 µm. Vertical bars represent means and error bars represent standard error. Significance values are represented as follows: "*" for $p = .05$.

has previously been observed in liver cells exposed to ethyl-parathion where Edwards *et al.* (2013) concluded that the MDA formation demonstrated that the lipid peroxidation was an auto-catalytic process caused by oxygen free radicals. Thus, the increase of MDA level in our study is consistent with the potential for ethyl-parathion-induced formation of ROS leading to lipid peroxidation in the SH-SY5Y cells. Consistent with our findings, OP exposures, including methyl-parathion, have been observed to cause increased lipid peroxidation in rat brain tissues (Canales-Aguirre *et al.*, 2012; Ojha *et al.*, 2011), as well as in liver, kidney, and spleen (Kalender *et al.*, 2005; Ojha *et al.*, 2011; Sulak *et al.*, 2005). Although the AChE inhibition mechanism of OP toxicity has been known for well over 50 years (Namba, 1971), the connection of this mechanism to oxidative-stress-related lipid-peroxidation and neurotoxicity is still not firmly established. A literature review by Pearson and Patel (2016) identified multiple observations that the severity of neuronal oxidative damage (lipid peroxidation) in rodents and humans correlated with increasing inhibition of AChE. However, they hypothesized that the relationship between AChE inhibition and oxidative stress induction may not be directly linked; sympathetic stimulation of glutamatergic pathways in OP exposures may stimulate ROS through NMDA receptor activation of nitric oxide synthesis as well as calcium influx into cells. Regardless of the mechanism,

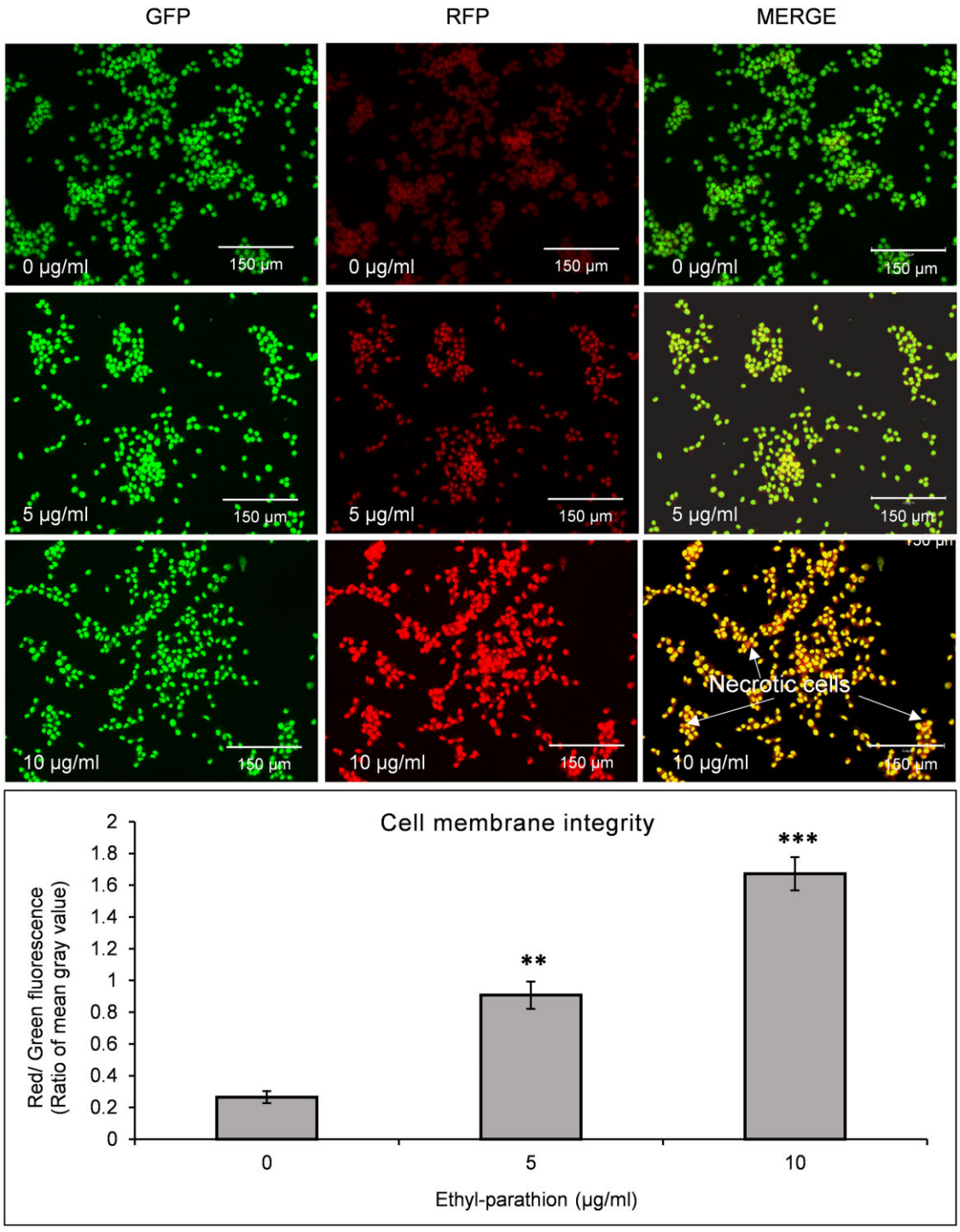

Figure 5. Effect of ethyl-parathion exposure on apoptosis in SH-SY5Y as determined by fluorescence imaging analysis of acridine orange (AO–GFP filter) and ethidium bromide (EB–RFP Filter) double-staining. Scale bar on image: 150 µm. Vertical bars represent mean fluorescence values and error bars represent standard error. Significance values are represented as follows: "*" for $p = .05$, "**" for $p = .01$, "***" for $p = .001$.

our results indicated the potential for ethyl-parathion exposures to induce lipid peroxidation in SH-SY5Y cells (Figure 3), most likely resulting from increased ROS formation (Figure 2).

Decreased mitochondrial membrane potential

Ethyl-parathion exposures elicited dose-dependent impacts on mitochondrial membrane status in the undifferentiated SH-SY5Y cells with significant effects occurring at 10 µg/ml (Figure 4). These results correspond to previous investigations of parathion exposure in SH-SY5Y cells where hyper-polarization of mitochondrial membranes were observed leading to decreasing overall mitochondrial function (Carlson and Ehrich, 1999). Further, mitochondrial dysfunction observed in investigations of rat N2a neuroblastoma cell exposures to the OP malathion were implicated as a noncholinergic mechanism leading to apoptotic cell death (Venkatesan *et al.*, 2017). A recent comprehensive literature review by Farkhondeh *et al.* (2020) concluded that OP-induced neurotoxicity was the result of a toxicity pathway initiated by OP-

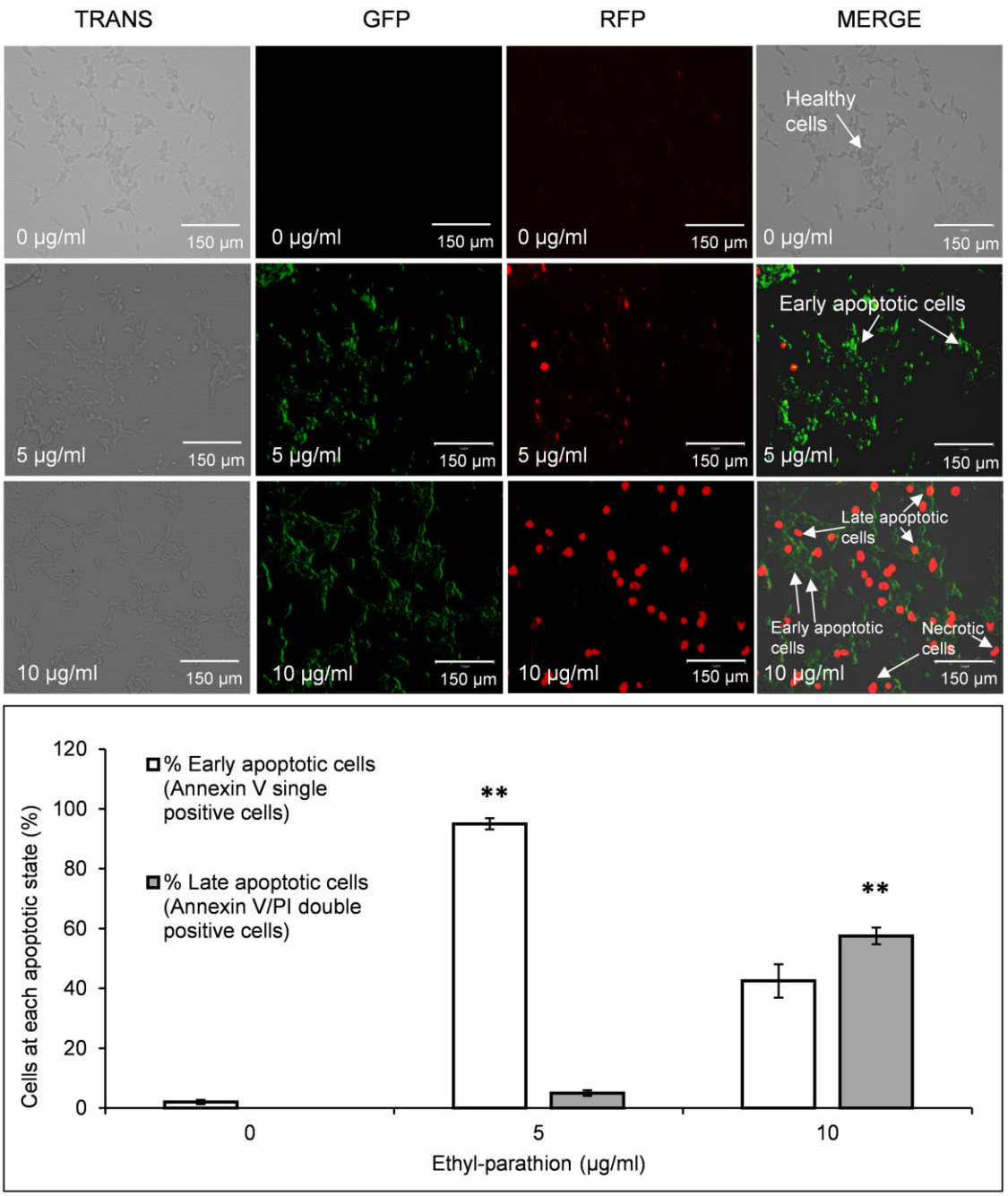

Figure 6. Effect of ethyl-parathion exposure on apoptosis in SH-SY5Y cells as determined by immunofluorescence imaging of cells stained with Annexin V-FITC/PI. TRANS indicates transmitted light microscopy, whereas GFP filter is for the Annexin V staining and RFP filter is for PI staining. Stages of apoptosis were determined as follows: double-negative staining represents no apoptosis, single-positive Annexin V staining representing early apoptosis, and double-positive stained cells are representative of cells in stages of late apoptosis. Scale bar on image: 150 µm. Vertical bars represent mean values for cells exhibiting signs of early and late apoptosis with error bars representing standard errors. Early and late apoptotic states were analyzed separately. Significance values are represented as follows: "*" for $p = .05$ and "**" for $p = .01$, where comparisons are made only among like-colored bars.

induced stimulation of cholinergic and glutamatergic signaling pathways; eliciting ROS and disrupting mitochondrial function in a positive feedback loop that further expands ROS release and calcium release into cells, ultimately inducing apoptosis mechanisms leading to cell death. At the whole-organism level, this OP neurotoxicity pathway has been implicated as a likely stimulus for several neurological disorders including depression, Parkinson's disease, and Alzheimer's disease (Farkhondeh *et al.*, 2020).

Apoptosis processes

Observations of ethyl-parathion-induced oxidative stress, lipid peroxidation, and decreased mitochondrial function in undifferentiated SH-SY5Y cells raised concerns that apoptotic processes may be initiated in compromised cells. In the present study, apoptotic cells were significantly increased in both the 5 and 10 µg/ml ethyl-parathion exposures relative to controls (Figure 5). Carlson *et al.* (2000) also observed significant induction of apoptosis in SH-SY5Y cells exposed to parathion and paraoxon, though

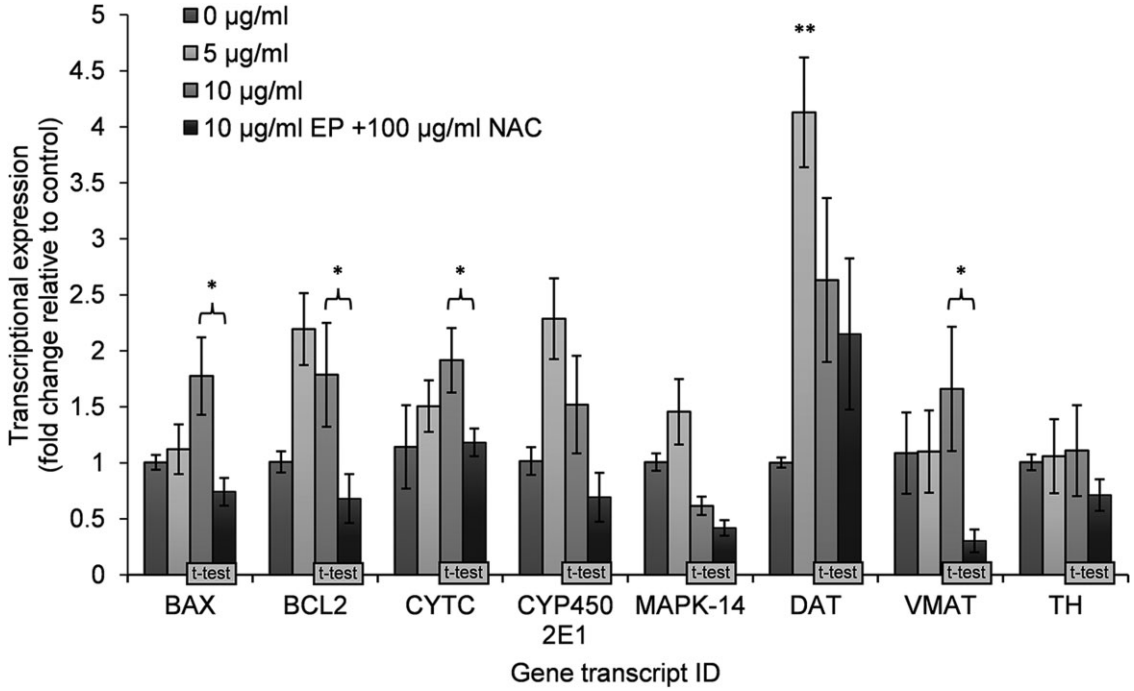

Figure 7. Effect of ethyl-parathion exposure on mRNA expression of BAX, BCL2, CYTC, CYP450-2E1, MAPK-14, DAT, VMAT, and TH in SH-SY5Y cells. The treatment named "10 µg/ml EP + 100 µg/ml NAC" represents the 10 µg/ml exposure to ethyl-parathion followed by addition of the ROS inhibitor N-acetyl L-cysteine (NAC 100 µg/ml). Vertical bars represent mean fold changes relative to controls, whereas error bar represents standard errors.

exposed at 1 mM (263.2 µg/ml) concentrations which are much higher than in the present study. In the present study, the proportion of early- to late-stage apoptotic cells significantly increased in the SH-SY5Y cells exposed to 5 µg/ml versus 10 µg/ml (Figure 6) indicating dose-dependent increases in sensitivity to ethyl-parathion. Venkatesan *et al.* (2017), investigated Malathion neurotoxicity in N2a mouse neuroblastoma cells and concluded that cellular apoptosis is likely a generalizable consequence of OP exposure/toxicity. Neuronal-cell apoptosis in response to OP exposure has also been confirmed *in vivo* where Canales-Aguirre *et al.* (2012) observed apoptosis in hippocampal neurons of rats exposed to parathion via inhalation (Canales-Aguirre *et al.*, 2012). In total, these apoptosis results for ethyl-parathion exposures in SH-SY5Y cells provide diagnostic endpoints typical of expected neurotoxic responses to OP exposures in neuronal tissues *in vivo*.

Transcriptomic expression

Overall, only one gene transcript, the dopamine active transporter (DAT), from the suite of 8 apoptosis and neurotoxicity-related gene targets surveyed in RT-qPCR assays showed a significant difference in the ethyl-parathion exposures relative to the controls. DAT expression had a nonmonotonic relationship with ethyl-parathion dose (Figure 7). Trends of increasing expression in response to the ethyl-parathion exposure were observed for many of the gene targets, but the results were not statistically significant where high variance in transcriptional expression was observed across all genes. The lack of statistical resolving power across the gene set makes interpretation of any nonsignificant trends tenuous and, therefore, were not included as part of our overall results interpretation. Future studies investigating these transcriptional targets in SH-SY5Y cells should include increased replication to reduce variance and increase statistical power.

DAT, the transcript that had significantly increased expression in the ethyl-parathion exposure (Figure 7), is a cell membrane-spanning protein that transports the neurotransmitter, dopamine, from the inter-neuronal synaptic cleft into the neuronal cytosol (Lohr *et al.*, 2017). OPs have been observed to interfere with dopamine signaling in mammalian neurophysiological systems (Torres-Altoro *et al.*, 2011). *In vivo* investigation of paraoxon (parathion-oxon) administration to intrastriatal neurons in conscious and freely moving rats by Alfonso *et al.* (2019) identified increased dopamine release via mechanisms independent of DAT-transporter action including vesicular-, Ca^{+2}-, and depolarization-dependent action. With this context, the effects of ethyl-parathion on the transcriptional expression of DAT observed in the present study suggest some potential for interference with dopaminergic signaling in SH-SY5Y cells, though the involvement of DAT to this response is presently unclear.

Conclusion

The present *in vitro* investigation of ethyl-parathion exposure in undifferentiated human SH-SY5Y cells demonstrated multiple cellular and molecular responses characteristic of OP neurotoxicity pathways observed in *in vivo* mammalian studies from the literature cited-herein. The strategic testing of ROS-generation/oxidative stress, lipid-peroxidation, MMP, and the progression of apoptosis status in the undifferentiated SH-SY5Y cells provided a very comprehensive evaluation of the principal toxicological cascade known to result in OP-induced neurotoxicity pathway. Characteristic of OPs, ethyl-parathion-induced generation of ROS (Figure 2) which corresponded with membrane-lipid peroxidation in undifferentiated SH-SY5Y cells (Figure 3). Consistent with *in vivo* responses, lipid-peroxidation has been observed to initiate a cascade of effects on mitochondrial function (Figure 4),

exacerbating oxidative stress, and inducing cellular apoptosis mechanisms (Figures 5 and 6). Overall, the molecular, subcellular, and cell viability (Figure 1) responses observed in the undifferentiated SH-SY5Y cells occurred at ethyl-parathion exposure concentrations that correspond well with mammalian *in vivo* exposure levels. Taken in total, the present study provides a successful demonstration of a high-fidelity nonanimal methodological approach for providing detailed mechanistic screening of characteristic mammalian OP neurotoxicity.

Acknowledgments

The authors thank Ms. Natalie Barker and Ms. Anne Mayo for assistance with materials acquisition and facilities management.

Funding

This work was supported by US Army Futures Command-funded 6.2-6.3 research program titled, "Understanding the Environment as a Threat," which is administered under the US Army, Engineer Research and Development Center's Installations and Operational Environments Technical Area.

Declaration of conflicting interests

The authors declared no potential conflicts of interest with respect to the research, authorship, and/or publication of this article.

References

Alfonso, M., Durán, R., Fajardo, D., Justo, L., and Faro, L. R. F. (2019). Mechanisms of action of paraoxon, an organophosphorus pesticide, on in vivo dopamine release in conscious and freely moving rats. *Neurochem. Int.* **124**, 130–140.

Amar, S. K., Goyal, S., Dubey, D., Srivastav, A. K., Chopra, D., Singh, J., Shankar, J., Chaturvedi, R. K., and Ray, R. S. (2015). Benzophenone 1 induced photogenotoxicity and apoptosis via release of cytochrome c and Smac/DIABLO at environmental UV radiation. *Toxicol. Lett.* **239**, 182–193.

Ankley, G. T., Bennett, R. S., Erickson, R. J., Hoff, D. J., Hornung, M. W., Johnson, R. D., Mount, D. R., Nichols, J. W., Russom, C. L., Schmieder, P. K., *et al.* (2010). Adverse outcome pathways: a conceptual framework to support ecotoxicology research and risk assessment. *Environ. Toxicol. Chem.* **29**, 730–741.

Argentin, G., Divizia, M., and Cicchetti, R. (2015). Oxidative stress, cytotoxicity, and genotoxicity induced by methyl parathion in human gingival fibroblasts: protective role of epigallocatechin-3-gallate. *J. Toxicol. Environ. Health. A* **78**, 1227–1240.

Audo, R., Hua, C., Hahne, M., Combe, B., Morel, J., and Daien, C. I. (2017). Phosphatidylserine outer layer translocation is implicated in IL-10 secretion by human regulatory B cells. *PLoS One* **12**, e0169755.

Bharate, S. B., Prins, J. M., George, K. M., and Thompson, C. M. (2010). Thionate versus Oxon: comparison of stability, uptake, and cell toxicity of $(14CH_3O)_2$-labeled methyl parathion and methyl paraoxon with SH-SY5Y cells. *J. Agric. Food Chem.* **58**, 8460–8466.

Brauchle, E., Thude, S., Brucker, S. Y., and Schenke-Layland, K. (2014). Cell death stages in single apoptotic and necrotic cells monitored by Raman microspectroscopy. *Sci. Rep.* **4**, 4698.

Canales-Aguirre, A. A., Gomez-Pinedo, U. A., Luquin, S., Ramírez-Herrera, M. A., Mendoza-Magaña, M. L., and Feria-Velasco, A. (2012). Curcumin protects against the oxidative damage induced by the pesticide parathion in the hippocampus of the rat brain. *Nutr. Neurosci.* **15**, 62–69.

Carlson, K., and Ehrich, M. (1999). Organophosphorus compound-induced modification of SH-SY5Y human neuroblastoma mitochondrial transmembrane potential. *Toxicol. Appl. Pharmacol.* **160**, 33–42.

Carlson, K., Jortner, B. S., and Ehrich, M. (2000). Organophosphorus compound-induced apoptosis in SH-SY5Y human neuroblastoma cells. *Toxicol. Appl. Pharmacol.* **168**, 102–113.

Dai, H., Deng, Y., Zhang, J., Han, H., Zhao, M., Li, Y., Zhang, C., Tian, J., Bing, G., and Zhao, L. (2015). PINK1/Parkin-mediated mitophagy alleviates chlorpyrifos-induced apoptosis in SH-SY5Y cells. *Toxicology* **334**, 72–80.

Edwards, F. L., Yedjou, C. G., and Tchounwou, P. B. (2013). Involvement of oxidative stress in methyl parathion and parathion-induced toxicity and genotoxicity to human liver carcinoma ($HepG_2$) cells. *Environ. Toxicol.* **28**, 342–348.

Faria, J., Barbosa, J., Queirós, O., Moreira, R., Carvalho, F., and Dinis-Oliveira, R. J. (2016). Comparative study of the neurotoxicological effects of tramadol and tapentadol in SH-SY5Y cells. *Toxicology* **359–360**, 1–10.

Farkhondeh, T., Mehrpour, O., Forouzanfar, F., Roshanravan, B., and Samarghandian, S. (2020). Oxidative stress and mitochondrial dysfunction in organophosphate pesticide-induced neurotoxicity and its amelioration: a review. *Environ. Sci. Pollut. Res. Int.* **27**, 24799–24814.

Goyal, S., Amar, S. K., Dwivedi, A., Mujtaba, S. F., Kushwaha, H. N., Chopra, D., Pal, M. K., Singh, D., Chaturvedi, R. K., Ray, R. S., *et al.* (2016). Photosensitized 2-amino-3-hydroxypyridine-induced mitochondrial apoptosis via Smac/DIABLO in human skin cells. *Toxicol. Appl. Pharmacol.* **297**, 12–21.

Gust, K. A., Ji, Q., and Luo, X. (2020). Example of adverse outcome pathway concept enabling genome-to-phenome discovery in toxicology. *Integr. Comp. Biol.* **60**, 375–384.

Gust, K. A., Wilbanks, M. S., Collier, Z. A., Burgoon, L. D., and Perkins, E. J. (2019). Adverse Outcome Pathway on antagonist binding to PPARα leading to body-weight loss. *OECD Series on Adverse Outcome Pathways, No. 10*. OECD Publishing, Paris.

Heusinkveld, H. J., and Westerink, R. H. S. (2017). Comparison of different in vitro cell models for the assessment of pesticide-induced dopaminergic neurotoxicity. *Toxicol. In Vitro* **45**, 81–88.

Judson, R. S., Houck, K. A., Kavlock, R. J., Knudsen, T. B., Martin, M. T., Mortensen, H. M., Reif, D. M., Rotroff, D. M., Shah, I., Richard, A. M., *et al.* (2010). In vitro screening of environmental chemicals for targeted testing prioritization: the ToxCast Project. *Environ. Health Perspect.* **118**, 485–492.

Kalender, S., Ogutcu, A., Uzunhisarcikli, M., Açikgoz, F., Durak, D., Ulusoy, Y., and Kalender, Y. (2005). Diazinon-induced hepatotoxicity and protective effect of vitamin E on some biochemical indices and ultrastructural changes. *Toxicology* **211**, 197–206.

Kovalevich, J., and Langford, D. (2013). Considerations for the use of SH-SY5Y neuroblastoma cells in neurobiology. *Methods Mol. Biol.* **1078**, 9–21.

Livak, K. J., and Schmittgen, T. D. (2001). Analysis of relative gene expression data using real-time quantitative PCR and the 2(-Delta Delta C (T)) Method. *Methods* **25**, 402–408.

Lohr, K. M., Masoud, S. T., Salahpour, A., and Miller, G. W. (2017). Membrane transporters as mediators of synaptic dopamine dynamics: implications for disease. *Eur. J. Neurosci.* **45**, 20–33.

Monnet-Tschudi, F., Zurich, M.-G., Schilter, B., Costa, L. G., and Honegger, P. (2000). Maturation-dependent effects of chlorpyrifos and parathion and their oxygen analogs on acetylcholinesterase

and neuronal and glial markers in aggregating brain cell cultures. *Toxicol. Appl. Pharmacol.* **165**, 175–183.

Mosmann, T. (1983). Rapid colorimetric assay for cellular growth and survival: applications to proliferation and cytotoxicity assays. *J. Immunol. Methods* **65**, 55–63.

Mylonas, C., and Kouretas, D. (1999). Lipid peroxidation and tissue damage. *In Vivo* **13**, 295–309.

Namba, T. (1971). Cholinesterase inhibition by organophosphorus compounds and its clinical effects. *Bull. World Health Organ.* **44**, 289–307.

Ojha, A., Yaduvanshi, S. K., and Srivastava, N. (2011). Effect of combined exposure of commonly used organophosphate pesticides on lipid peroxidation and antioxidant enzymes in rat tissues. *Pestic. Biochem. Physiol.* **99**, 148–156.

Pearson, J. N., and Patel, M. (2016). The role of oxidative stress in organophosphate and nerve agent toxicity. *Ann. N. Y. Acad. Sci.* **1378**, 17–24.

Piña-Guzmán, B., Sanchez-Gutierrez, M., Marchetti, F., Hernandez-Ochoa, I., Solis-Heredia, M. J., and Quintanilla-Vega, B. (2009). Methyl-parathion decreases sperm function and fertilization capacity after targeting spermatocytes and maturing spermatozoa. *Toxicol. Appl. Pharmacol.* **238**, 141–149.

Ranjbar, A., Pasalar, P., and Abdollahi, M. (2002). Induction of oxidative stress and acetylcholinesterase inhibition in organophosphorus pesticide manufacturing workers. *Hum. Exp. Toxicol.* **21**, 179–182.

Richard, A. M., Judson, R. S., Houck, K. A., Grulke, C. M., Volarath, P., Thillainadarajah, I., Yang, C., Rathman, J., Martin, M. T., Wambaugh, J. F., *et al.* (2016). ToxCast chemical landscape: paving the road to 21st century toxicology. *Chem. Res. Toxicol.* **29**, 1225–1251.

Sala, G., Marinig, D., Riva, C., Arosio, A., Stefanoni, G., Brighina, L., Formenti, M., Alberghina, L., Colangelo, A. M., and Ferrarese, C. (2016). Rotenone down-regulates HSPA8/hsc70 chaperone protein in vitro: a new possible toxic mechanism contributing to Parkinson's disease. *Neurotoxicology* **54**, 161–169.

Schneider, C., Rasband, W., and Eliceiri, K. (2012). NIH Image to ImageJ: 25 years of image analysis. *Nat. Methods.* **9**, 671–675.

Sulak, O., Altuntas, I., Karahan, N., Yildirim, B., Akturk, O., Yilmaz, H. R., and Delibas, N. (2005). Nephrotoxicity in rats induced by organophosphate insecticide methidathion and ameliorating effects of vitamins E and C. *Pestic. Biochem. Physiol.* **83**, 21–28.

Torres-Altoro, M. I., Mathur, B. N., Drerup, J. M., Thomas, R., Lovinger, D. M., O'Callaghan, J. P., and Bibb, J. A. (2011). Organophosphates dysregulate dopamine signaling, glutamatergic neurotransmission, and induce neuronal injury markers in striatum. *J. Neurochem.* **119**, 303–313.

United States Environmental Protection Agency (USEPA). Organophosphate pesticide information: Overview of the ethyl parathion revised risk assessment (EPA-738-F00-009). September 2000. Available at: https://www3.epa.gov/pesticides/chem_search/reg_actions/reregistration/fs_PC-057501_1-Sep-00.pdf.

Venkatesan, R., Park, Y. U., Ji, E., Yeo, E.-J., and Kim, S. Y. (2017). Malathion increases apoptotic cell death by inducing lysosomal membrane permeabilization in N2a neuroblastoma cells: a model for neurodegeneration in Alzheimer's disease. *Cell Death Discov.* **3**, 17007.

Zhao, Q., Yang, X., Cai, D., Ye, L., Hou, Y., Zhang, L., Cheng, J., Shen, Y., Wang, K., and Bai, Y. (2016). Echinacoside protects against MPP (+)-induced neuronal apoptosis via ROS/ATF3/CHOP pathway regulation. *Neurosci. Bull.* **32**, 349–362.